专题评述

DOI: 10.15541/jim20230453

MXenes 及其复合物的太赫兹电磁屏蔽与吸收

万胡杰[1,2], 肖 旭[1]

(电子科技大学 1. 物理学院, 电子薄膜与集成器件全国重点实验室; 2. 电子科学与工程学院, 成都 611731)

摘 要: 开发新型低维材料在太赫兹电磁屏蔽与吸收领域的应用是一个极为重要的研究方向, 低维材料以其独特的电学、力学与电磁响应而有望创造出更加高效的电磁屏蔽与吸收方案。二维过渡金属碳化物、氮化物与碳氮化合物 MXenes 在低频波段已经展示出优异的电磁屏蔽与吸收性能, 尤其是 MXenes 兼具高电导率、低密度、高柔性等特点, 有利于未来太赫兹器件便携化与系统集成化。然而, 将 MXenes 太赫兹电磁屏蔽与吸收材料推向实际应用过程中, 面临着附着稳定性、环境稳定性、不耐高温等问题, 无法满足航空航天和第六代通信场景需求。此外，目前缺乏更加全面的太赫兹散射与吸收验证手段。针对上述问题，研究人员开展了广泛且深入的工作。本文回顾了近年来主流电磁屏蔽与吸收材料的主体构型与基础理论原理, 并重点介绍了多种 MXenes 及其复合物在薄膜与多孔结构下的太赫兹电磁屏蔽与吸收特性, 包括 $Ti_3C_2T_x$、$Mo_2Ti_2C_3T_x$、$Mo_2TiC_2T_x$、$Nb_4C_3T_x$、Nb_2CT_x, 并展望了 MXenes 作为太赫兹频段中电磁屏蔽与吸收材料所面临的挑战和机遇。

关 键 词: 二维材料; MXenes; 太赫兹; 电磁屏蔽与吸收材料; 专题评述

中图分类号: TN927 **文献标志码:** A **文章编号:** 1000-324X(2024)02-0129-16

Terahertz Electromagnetic Shielding and Absorbing of MXenes and Their Composites

WAN Hujie[1,2], XIAO Xu[1]

(1. State Key Laboratory of Electronic Thin Films and Integrated Devices, School of Physics, University of Electronic Science and Technology of China, Chengdu 611731, China; 2. School of Electronic Science and Engineering, University of Electronic Science and Technology of China, Chengdu 611731, China)

Abstract: Developing novel low-dimensional materials for terahertz electromagnetic shielding and absorbing applications represents a critical research frontier. Their unique electrical, mechanical, and electromagnetic responses hold great potential in enabling more efficient solutions for electromagnetic shielding and absorbing. Two-dimensional transition metal carbides, nitrides, and carbonitride MXenes have already demonstrated excellent electromagnetic shielding and absorbing performance in the low-frequency spectrum. MXenes possess high conductivity, low density, and high flexibility, which are advantageous for future portability and integration of terahertz devices and systems. However, practical implementation of MXene-based terahertz electromagnetic shielding and absorption materials faces challenges in adhesion stability, environmental resilience, and high-temperature tolerance, hindering their suitability

收稿日期: 2023-10-05; **收到修改稿日期:** 2023-12-23; **网络出版日期:** 2023-12-25

基金项目: 国家重点研发计划(2023YFB3811303); 四川省自然科学基金(2023NSFSC0437); 四川省科技支撑计划(2021JDTD0026)
National Key Research and Development Program of China (2023YFB3811303); Natural Science Foundation of Sichuan Province (2023NSFSC0437); Sichuan Science and Technology Support Program (2021JDTD0026)

作者简介: 万胡杰(1998–), 男, 博士研究生. E-mail: 202211022617@std.uestc.edu.cn
WAN Hujie (1998–), male, PhD candidate. E-mail: 202211022617@std.uestc.edu.cn

通信作者: 肖 旭, 研究员. E-mail: xuxiao@uestc.edu.cn
XIAO Xu, professor. E-mail: xuxiao@uestc.edu.cn

for aerospace and future next generation communication applications. Moreover, in the terahertz frequency band, lacking more comprehensive and reliable electromagnetic scattering and absorbing measurement methods limits the development of THz shielding and absorbing materials. Extensive research efforts have targeted on these limitations, exploring fundamental architectural and theoretical aspects of prevalent electromagnetic materials. This review specifically highlights the terahertz electromagnetic shielding and absorption characteristics inherent in various MXenes and their compositions, such as $Ti_3C_2T_x$, $Mo_2Ti_2C_3T_x$, $Mo_2TiC_2T_x$, $Nb_4C_3T_x$, and Nb_2CT_x. Additionally, this review envisages the forthcoming challenges and prospects of MXenes as a pivotal electromagnetic shielding and absorbing material within the terahertz frequency band.

Key words: two-dimensional material; MXenes; terahertz; electromagnetic shielding and absorbing material; perspective

太赫兹(THz)波是一种频率在 0.1~10 THz (波长: 0.03~3 mm)范围的电磁波, 在天文学[1-2]、信息与通信技术[3]、国土安全[4]、分子识别[5]、工业检测[6]、生物与医学成像[7]等重要领域都具有巨大的潜力。近年来, 太赫兹技术被确定为第六代通信技术(6G)的核心技术之一[8-10], 用以满足人工智能和物联网相结合时所需的大容量传输速率(100 Gbit/s)的需求[11-12]。随着太赫兹技术的不断发展, 太赫兹通信系统与雷达系统都进入了实用化发展阶段。太赫兹技术的高频与高带宽特性, 使得短距离数据传输速度提升至 160 Gbit/s[11], 而太赫兹雷达系统则主要应用于 215~240 GHz[13]、315~540 GHz[14-15]、1.5 THz[16]等频段, 在民用安检等领域有广泛应用。尽管太赫兹技术具有巨大的应用潜力, 但是相关的电子设备与工业设施所产生的太赫兹旁瓣信号会不可避免地干扰邻近的电子电路或精密电子设备, 如微型生物植入芯片、太赫兹探测器、太赫兹全息通信系统、太赫兹自由空间系统等[8, 17-19]。因此, 研究太赫兹屏蔽及吸收材料对于电磁防护、信息保密、国防安全等领域具有极其重要的研究意义。传统的金属材料(Cu, Al, Ag)在电磁屏蔽与吸收方面发挥着重要作用, 但是高密度、难加工、高腐蚀敏感性限制了它们在高度集成的现代信息设备中的应用[20]。目前, 由各类导电填料, 例如, 碳纳米管、石墨烯、氧化石墨烯等[21-25], 组成的复合物被广泛作为电磁屏蔽与吸收材料, 用于替代传统金属材料。这些复合物大多轻质、环境稳定性更好, 但其电磁屏蔽效率相对较低, 又限制了它们的广泛应用。

MXenes 包括二维过渡金属碳化物、氮化物和碳氮化物, 其一般化学式为 $M_{n+1}X_nT_x$, 其中 n=1、2、3 或 4; M 为过渡金属, 如钛、钒、铌、钼、钪、钇、锆、铪、钽、铬、钨等; X 为碳和/或氮; T_x 为表面修饰基团, 如–OH、=O、=S、–F、–Cl、–Br、–Se、–NH、–Te 等[20, 26-27]。目前, MXenes 的主流合成方式仍是通过对三元碳化物 MAX 化合物进行选择性蚀刻, 去除 A 族元素(如 Al、Si 或 Ga 等)后得到, 例如, 从 Ti_3AlC_2 得到 Ti_3C_2[28]。这类材料自 2011 年发现以来[29], 已经有 100 多种理论上可能的 MXenes 组合, 其结构框架如图 1 所示, 其中 M 位代表过渡金属原子, 其在平面内和垂直于平面方向可有序或无序排列, 同时 C 和/或 N 原子皆可占据 X 位, 各种表面修饰基团(取决于蚀刻和/或剥离条件)的不同组合方式, 构成了不同类型 MXenes, 呈现出多样的物理与化学特性。与其他大多数二维材料相比, $Ti_3C_2T_x$ MXene 以其高导电性、亲水性、超薄特性以及近全太赫兹频段均一电导特性而备受关注。它在太赫兹电磁屏蔽与吸收方面表现出色, 在太赫兹波段各种电子和光电领域具有巨大应用潜力[30-31]。

本专题评述将从太赫兹波段电磁屏蔽与吸收机制、MXenes 及其复合物层状薄膜与 MXenes 多孔吸

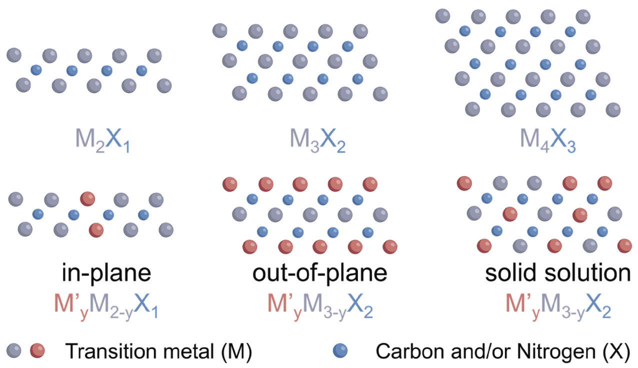

图 1 MXenes 的结构示意图

Fig.1 Chemical structures of MXenes

2D MXenes have a general formula of $M_{n+1}X_nT_x$, where M is an early transition metal, X is carbon and/or nitrogen, and T_x represents surface terminations of the outer metal layers. The n value in the formula can vary from 1 to 4, depending on the number of transition metal layers (and carbon and/or nitrogen layers) present in the structure of MXenes, for example, Ti_2CT_x (n = 1), $Ti_3C_2T_x$ (n = 2), $Nb_4C_3T_x$ (n = 3), and $(Mo,V)_5C_4T_x$ (n = 4)

波体的太赫兹电磁屏蔽与吸收特性等方面出发，介绍近年来 MXenes 在太赫兹领域的研究进展，并总结太赫兹频段 MXenes 的电磁屏蔽与吸收特性。

1 太赫兹屏蔽与吸波机制

对于电磁屏蔽材料，当电磁波入射后会与材料中的导电性物质相互作用，使得绝大部分入射信号无法穿透样品。材料吸收与反射信号都有助于提升电磁屏蔽效能(Electromagnetic Interference Shielding Efficiency, EMI SE)，然而，未被吸收的反射电磁波仍会干扰周围的精密电子设备[32]。

针对电磁吸收材料，其本征吸收损耗主要是指电磁波在媒质中传播时所引起的功率密度衰减，包括导电损耗、极化弛豫、磁损耗、多重反射损耗等。其中在太赫兹频段，磁损耗较难实现，这是由于传统铁磁材料的磁化谐振频率大多处于吉赫兹(GHz)频段，只有极少部分反铁磁材料，如 $BiFeO_3$、$YFeO_3$ 等[33-34]，能在太赫兹波段由电子自旋共振(Electron Spin Resonance)引起较强的磁响应。因此，目前已报道的太赫兹自然吸波材料的本征损耗主要以传导损耗与极化弛豫为主。

相对于自然吸波材料，人工超材料通过设计特定的单元结构阵列(Split-ring resonators, SRRs)可以引入强烈的电和磁的谐振损耗[35-36]。利用材料本身的电磁参数和特定结构设计，人工超材料能够实现高效的电磁屏蔽与吸收特性。以下是几种典型的电磁屏蔽与吸收构型(表 1)[37-38]。

1.1 Salisbury 屏吸波体[39]

Salisbury 屏结构是一种谐振式的窄带吸收体(图 2(a))，主要结构为阻抗等于空气阻抗的金属层，厚度为 1/4 介质波长奇数倍的低介电常数介质层与金属全反射层。通过介质层厚度带来的波程差实现干涉相消进行损耗吸收。Salisbury 屏结构作为主流的损耗构型，近年来广泛用于超材料吸收体，增强谐振吸收和带宽[40-41]。

表 1　太赫兹电磁屏蔽与吸收机制[37-38]

Table 1　Terahertz electromagnetic shielding and absorption mechanism[37-38]

Classification	Absorbing mechanism	Remark
Salisbury screen 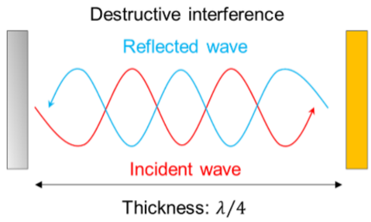	A resistive sheet is placed $\lambda_0/4$ in front of a metal ground plane, usually separated by some lossless dielectrics. The reflectivity drops to zero due to destructive interference between the scattering paths in the device.	(a) Narrow band (b) Destructive interference (c) Easy to process
Jaumann absorber 	The Jaumann absorber, an extension of the Salisbury screen, primarily comprises multiple thin impedance layers, lossless dielectric layers, and a metal layer. The electromagnetic characteristics of each impedance layer and the thickness of the dielectric layer are designed to operate at distinct frequencies, enabling destructive interference absorption across multiple frequency points and achieving broadband absorption.	(a) Broadband frequency (b) Destructive interference (c) Substantial thickness and intricate processing methods
Dällenbach absorber 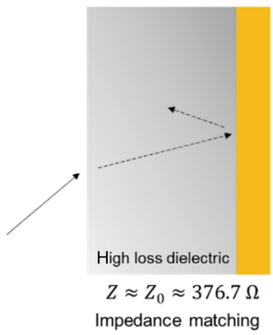	The impedance matching layer is designed for specific high imaginary part of dielectric constant and permeability, while matching the free-space impedance.	(a) High imaginary part of dielectric constant and permeability ε'', μ'' (b) Free-space impedance matching (c) The absorption bandwidth is related to the conduction-frequency characteristics (d) Easy to process

续表

Classification	Absorbing mechanism	Remark
Impedance gradient multilayer absorber  Graded impedance	Similar to the Dällenbach absorber, the layer-by-layer impedance matching design minimizes the reflected component of the interface when waves are incident.	(a) Gradient interface impedance matching (b) The absorption bandwidth is related to the conduction-frequency characteristics (c) Complicated process
Pyramidal type absorber 	The pyramidal-type absorber, an evolution from the Dällenbach absorber framework, adopts a specific angle design to maximize incident wave capture, minimizing reflection. Electromagnetic waves undergo multiple reflections along the cone structure. Both pyramidal and tetrahedral pyramidal configurations exhibit reduced demands concerning the polarization direction of electromagnetic waves.	(a) The macrostructure captures the incident wave and reduces scattering (b) The absorption bandwidth is related to the conduction-frequency characteristics (c) Easy to process
Metamaterial absorber 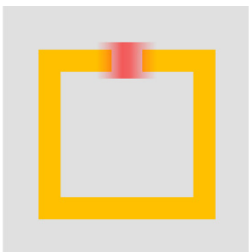	The resonant response exhibited by distinctive metamaterial structure serves the purpose of dissipating incident electromagnetic waves. Owing to the notably high degree of freedom within this characteristic structure, metamaterials can be engineered for either single-frequency or wide-band resonant absorption. To achieve broadband absorption, multiple distinct single-frequency resonant structures are employed and combined. However, due to practical limitations in the manufacturing process, there remains a gap in absorption between the multiple resonant frequencies, leading to partial absorption within specific frequency bands.	(a) Electromagnetic resonance characteristic structure (b) Adjustable electromagnetic parameters (ε,μ) (c) The processing difficulty is related to the wavelength
Coherent perfect absorber 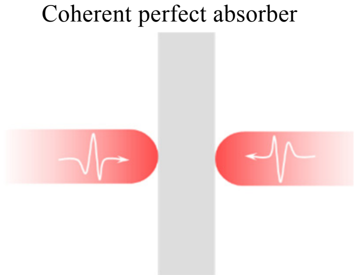	When two normal incidence plane waves with an odd times π phase difference enter the impedance layer from both ends, interference cancelation occurs, and all electromagnetic waves will be absorbed.	(a) Coherent wave (b) Phase difference: $(2n+1)\pi$ (c) The absorption bandwidth is related to the conduction-frequency characteristics
Artificial blackbody 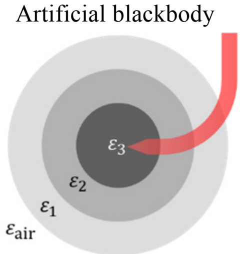 Graded dielectric constant	In the domain of artificial black holes, spheres and cylinders stand as prevalent design frameworks. Multi-layer spheres and cylinders are designed to increase the dielectric constant of the medium layer by layer from the outside to the inside. The center is full of material with high imaginary part of dielectric constant, and the incident wave is deflected to the center layer by layer and converges and loses.	(a) Gradient dielectric constant $\varepsilon(r)=\begin{cases}\varepsilon_0, r>R\\ \varepsilon_0\left(\frac{R}{r}\right)^2, R_c<r<R\\ \varepsilon_c+i\gamma, r<R_c\end{cases}$ (b) The overall geometry is larger than the wavelength diffraction limit

1.2 Dällenbach 吸波体[38]

如图 2(b)所示, Dällenbach 吸波体采用了不同于 Salisbury 屏的机制, 它包括一个均匀阻抗层与金属全反射层。均匀阻抗层由高介电常数和磁导率虚部材料构成, 产生特定的损耗值, 并调控阻抗匹配到自由空间阻抗, 以尽量减少表面反射, 并利用均匀层中的损耗来吸收入射电磁波。在太赫兹频段, Dällenbach 吸波体是目前应用最广泛的吸收体构型,

其阻抗层大多被设计为复合物多孔导电网络。

1.3 多层渐变阻抗匹配吸波体[38]

图2(c)显示，作为Dällenbach吸收体的扩展，高介电常数与磁导率虚部往往会造成阻抗匹配性能差，多层渐变阻抗匹配结构采用逐层减小等效阻抗的阻抗层，并尽可能地提高每层的电磁损耗，减少各界面间阻抗不匹配的反射，入射波由每层吸波材料进行损耗，对于给定材料范围、层数、总厚度和吸收频段等参数条件，可由神经网络算法、遗传算法等优化得到最优化吸波体的结构[42-43]。由于逐层设计加工难度较高，广泛应用的仍然是梯度填充质量分数渐变的导电填料的吸波体。

1.4 Jaumann 吸波体[38]

如图 2(d)所示，原理上可将 Jaumann 吸收器看作 Salisbury 屏的扩展，Salisbury 屏变为由单个金属反射层前的两个或多个阻抗层组成。所有的阻抗层薄片都被设计成在不同波长下工作，因此每个薄片之间的距离大约为$\lambda/4$，在对应中心频率 λ_0 附近产生多个反射最小值，从而作为多频点共振吸收器在多个波长实现宽带吸收响应。带宽会随着层数增加而增加，其吸波特性由各层的面电阻、层间间隔和间隔材料的电磁参数决定。然而，这会使 Jaumann 吸收器变得又厚又笨重，对于宽频 Jaumann 吸收体的结构优化，层数越多对应的优化复杂度越高。

1.5 锥体吸波体[44-45]

如图2(e)所示，基于Dällenbach吸波体，锥体吸波器在电磁波入射侧呈四面体锥状，利用宏观结构引导电磁波沿锥体多次反射损耗，因此该吸波器对两种极化方向的电磁波都具有宽频带内的电磁波吸收特性。通过电磁有限元仿真，可以完成相应的结构设计仿真验证。这种构型吸波器应用最为广泛，大多基于导电碳材料与铁磁材料浸渍聚氨酯泡沫、聚苯乙烯泡沫或类似材料制成。

1.6 超材料吸波体[37]

超材料体系通过设计特定的亚波长结构阵列(图 2(f))，SRRs、环形结构等效为电感，间隙等效电容)，同时对整体的介电常数 $\varepsilon(\omega)$ 和磁导率 $\mu(\omega)$ 进行调节，在满足阻抗匹配的条件下，主要利用亚波长结构的电磁谐振机制来实现电磁能到欧姆热的转化。单一谐振结构单元通常对应窄频吸收，因此大多宽频吸收超材料需要多种谐振单元组合工作。随着频段加宽，其结构的设计与加工也将变得更加复杂[46]。

1.7 相干完美吸波体[47-49]

传统的相干完美吸收器(Coherent perfect absorber, CPA)通过在两个平面镜之间放置一个临界耦合吸收器来吸收正入射的同频相位相差π的奇数倍平面波(图 2(g))。当满足相干完全吸收条件时，来自多次往返的所有反射会干涉相消，所有能量都被吸收。然而，对于以不同角度或以其他模式入射的任何其他输入场，多次往返的反射场不再具有相同的空间分布，吸收性能将会下降。根据 Woltersdorff 的研究，纳米尺度下金属薄膜具有 50%的吸收极限，且与入射电磁波无关，在相干完美吸波体结构中，中间放置薄膜阻抗等于空气阻抗的一半，即可完成超薄超宽带电磁吸收[50]。CPA 作为吸波材料构型对入射波要求极高，限制了其广泛应用，但CPA对入射波形的敏感特性为灵活控制光散射和吸收提供了机会[51]。

1.8 人工黑洞[52]

如图 2(h)所示，“人工黑洞”大多以球体和圆柱体为基础框架，设计为多层结构，从外到内调控层的介电常数逐层增加，使入射波逐层向中心偏转汇聚，内层材料设计为高介电常数虚部 γ 以帮助损耗入射波。这种方法不依赖于任何共振，并且能够在宽带下同时全向高吸收，其介电常数随半径变化如下:

$$\varepsilon(r)=\begin{cases}\varepsilon_0, r>R\\ \varepsilon_0\left(\dfrac{R}{r}\right)^2, R_c<r<R\\ \varepsilon_c+\mathrm{i}\gamma, r<R_c\end{cases} \tag{1}$$

其中，ε_0 和 ε_c 分别为自由空间介电常数和最内层介电常数，R 为人工黑洞最外层半径，r 为半径自变量，$R_c=R\sqrt{\varepsilon_0/\varepsilon_c}$ 为最内层的临界半径。

2　太赫兹电磁屏蔽与反射损耗测试原理

典型太赫兹电磁屏蔽性能与反射损耗性能测试如图 3 所示，电磁屏蔽性能公式为:

$$\text{EMI SE}=-20\lg(E_{sam}/E_{inc}) \tag{2}$$

E_{sam} 和 E_{inc} 分别代表样品透射电场信号和入射波穿过空气的电场信号。

反射损耗性能计算公式为:

$$\text{RL}=-20\lg(E_i/E_{ref}) \tag{3}$$

E_i 和 E_{ref} 分别代表样品反射电场信号和参考全反射金属铝/金的电场信号。在商用领域，通常反射损耗大于–10 dB 便能满足需求。

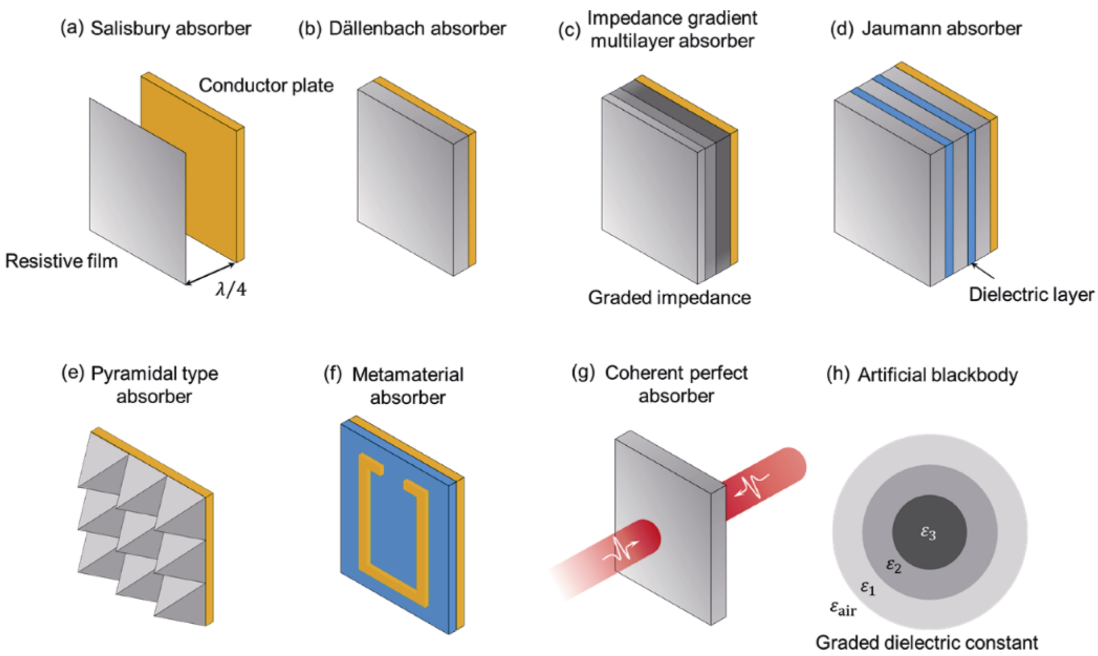

图 2 典型电磁吸收体的原理示意图

Fig. 2 Schematic illustration of electromagnetic absorber

(a) Salisbury screen absorber. The resistive film placed at 1/4 wavelength in front of the metal plate[39]; (b) Dällenbach absorber. The impedance of resistive film is equal to free space impedance to reduce reflection[38]; (c) Impedance gradient multilayer absorber. The impedance decreases layer by layer from large to small, reducing reflections while increasing conductive loss absorption[38]; (d) Jaumann absorber. All the layers are designed to operate at different wavelengths, so that the distance between each sheet is approximately $\lambda/4$, producing multiple reflection minima around some center frequency λ_0 [38]; (e) Pyramidal type absorber. Multiple reflection losses along the cone, so the absorber has a wide band of electromagnetic wave absorption characteristics for both polarization direction electromagnetic waves[44-45] ; (f) Metamaterial absorber. Electromagnetic resonance loss depends on subwavelength metal-structure[37]; (g) Coherent perfect absorber in free space[49]; (h) Artificial black holes consisting of multiple layers of asymptotically varying dielectric constant spheres and/or cylinders, with the dielectric constant increasing from outside to inside, from small to large[52]

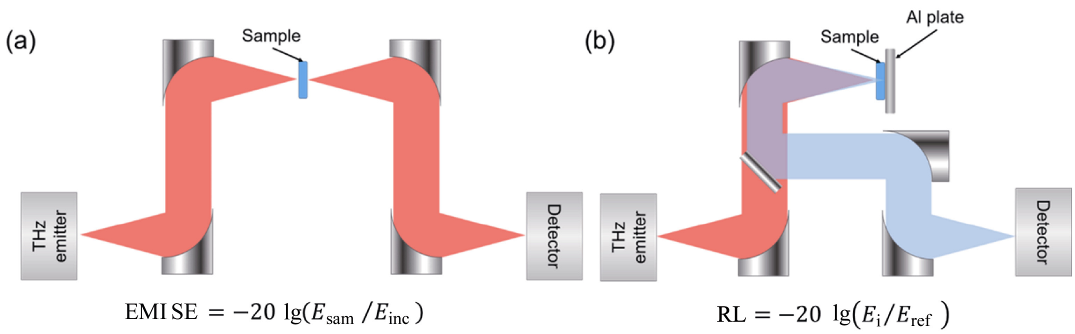

图 3 太赫兹电磁屏蔽效能(a)和反射损耗(b)测试原理图[57]

Fig. 3 Schematic illustration of a THz-TDS system for electromagnetic interference shielding efficiency (a) and reflection loss measurements (b)[57]

(Reprinted from Ref. [57] with permission, Copyright 2021, American Chemical Society)

以上两种测试方法适用于大多数均匀且平整表面样品，其中表面的粗糙度尺寸要远小于波长。然而，对于多孔或表面粗糙样品，需要利用积分球反射法[53]、雷达散射截面测试等技术采集散射信号，验证其吸收特性[52, 54-56]。需要指出的是，在太赫兹频段，多孔或者非均匀表面样品吸收测试设备还需进一步研发，以制定统一的测试标准。

3 MXenes 及其复合物层状薄膜

近年来，$Ti_3C_2T_x$ 作为电导率最高的 MXene 材料之一(1×10^4~2×10^4 S/cm)，在太赫兹电磁吸收与屏蔽领域受到了广泛关注。2018 年，Jhon 等[58]利用第一性原理计算指出在 0.3~1.9 THz 波段，单层和两

层 Ti_3C_2 表现出极高的吸收系数，分别为 70000~90000 和 45000~60000 cm^{-1}，计算还发现，当考虑自旋轨道耦合效应(Spin-orbit coupling)时几乎不会影响 Ti_3C_2 的吸收能力。同年，Choi 等[59]发现，将数十纳米厚的MXene薄膜与金纳米狭缝天线组合，能够极大增强MXene薄膜的太赫兹电磁屏蔽效能，消光比大约为1000倍。研究人员通过数值计算仿真，发现金纳米狭缝天线的太赫兹波强局域化，加强了太赫兹波与MXene的相互作用(如图4)，提高了MXene太赫兹探测器的响应能力。Titova 课题组[60-63]分别在 2019 年与 2020 年报道了 $Ti_3C_2T_x$、$Mo_2Ti_2C_3T_x$ 和 $Mo_2TiC_2T_x$ 的太赫兹与超快载流子动力学特性。研究人员利用Drude-Smith模型对以上三种MXenes的太赫兹电导特性($\sigma_{THz}(\omega)$)进行拟合(图 5)，MXenes 展现出极高的背散射系数(–0.6~–1)，极短的载流子弛豫时间(15~20 fs)。表 2 总结了已报道的MXenes的背散射系数与弛豫时间[60-62, 64-65]。基于唯象的 Drude-Smith 模型，研究人员将背散射与极短弛豫来源唯象地解释为杂质(官能团)散射、缺陷散射、晶界散射和边界散射。由于缺乏化学气相沉积(Chemical Vapor Deposition, CVD)合成单晶薄膜的手段，对于以上散射机制的讨论仍有一定困难。目前 MXenes 制备最常用的方法是湿化学蚀刻(HCl&HF、MILD)和熔融盐蚀刻($CuCl_2/ZnCl_2$)[66-68]，但不同的合成方法得到的 MXenes 的缺陷、层片尺寸、表面修饰基团和残余插层物皆会对 MXenes 的光子学和电学性能产生影响。例如，借助二次离子质谱(Secondary-Ion Mass Spectrometry, SIMS)分析过量铝修饰的 Ti_3AlC_2 和 $Ti_3C_2T_x$，发现碳层中的氧缺陷可以忽略不计，这可以显著提高 MXenes 的电导率[69]。然而，目前很难对表面官能团、缺陷、晶界、层间距和横向尺寸等参数进行系统调控，这

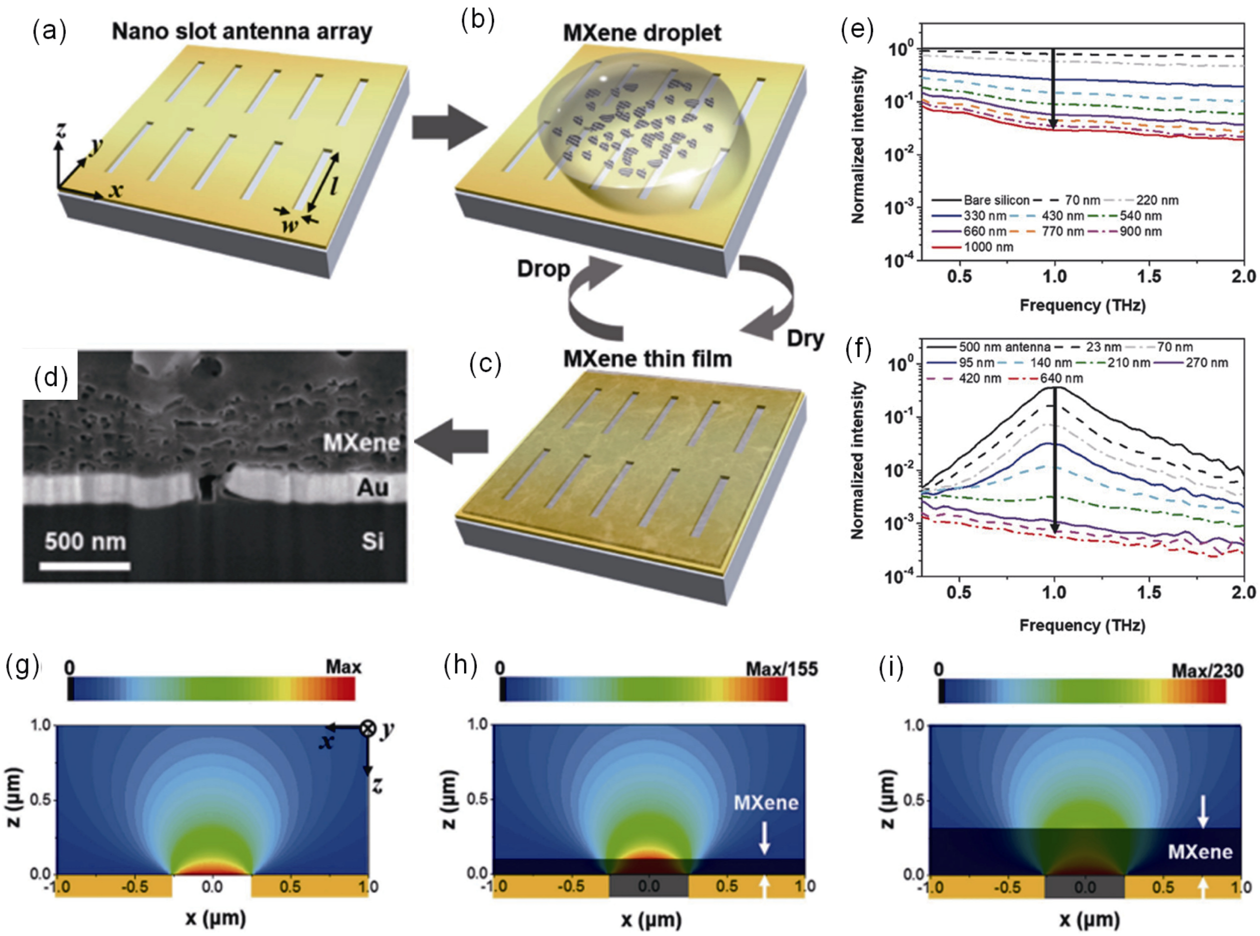

图 4　基于金纳米狭缝天线的 MXene 电磁屏蔽增强现象[59]

Fig. 4　Enhanced THz electromagnetic shielding phenomenon of MXene based on gold nano-slit antenna[59]

(a) Scheme of MXene-coated nano-metamaterial antennas; (b, c) Thin film of MXene made by drop-casting of MXene flakes followed by drying in air for many cycles to achieve the desirable thickness; (d) SEM image of the as-prepared MXene film with 150 nm width antenna; (e) Normalized transmittance spectra of the bare silicon and various thicknesses of MXene films on the silicon substrate; (f) Normalized transmittance spectra of the antenna and various thicknesses of MXene on the 500 nm width antenna array; Electric field intensity distributions of transmitted THz wave near the 500 nm width antenna, obtained by analytical calculation of antenna (g) without MXene, with (h) 100 nm thick MXene on the antenna and (i) 300 nm thick MXene on the antenna. The yellow and gray colors indicate the gold nano-slot antenna and MXene, respectively. In (h, i), the MXene filled the gap of the nano-antenna (Reprinted from Ref. [59] with permission, Copyright 2018, WILEY-VCH Verlag GmbH & Co. KGaA, Weinheim)

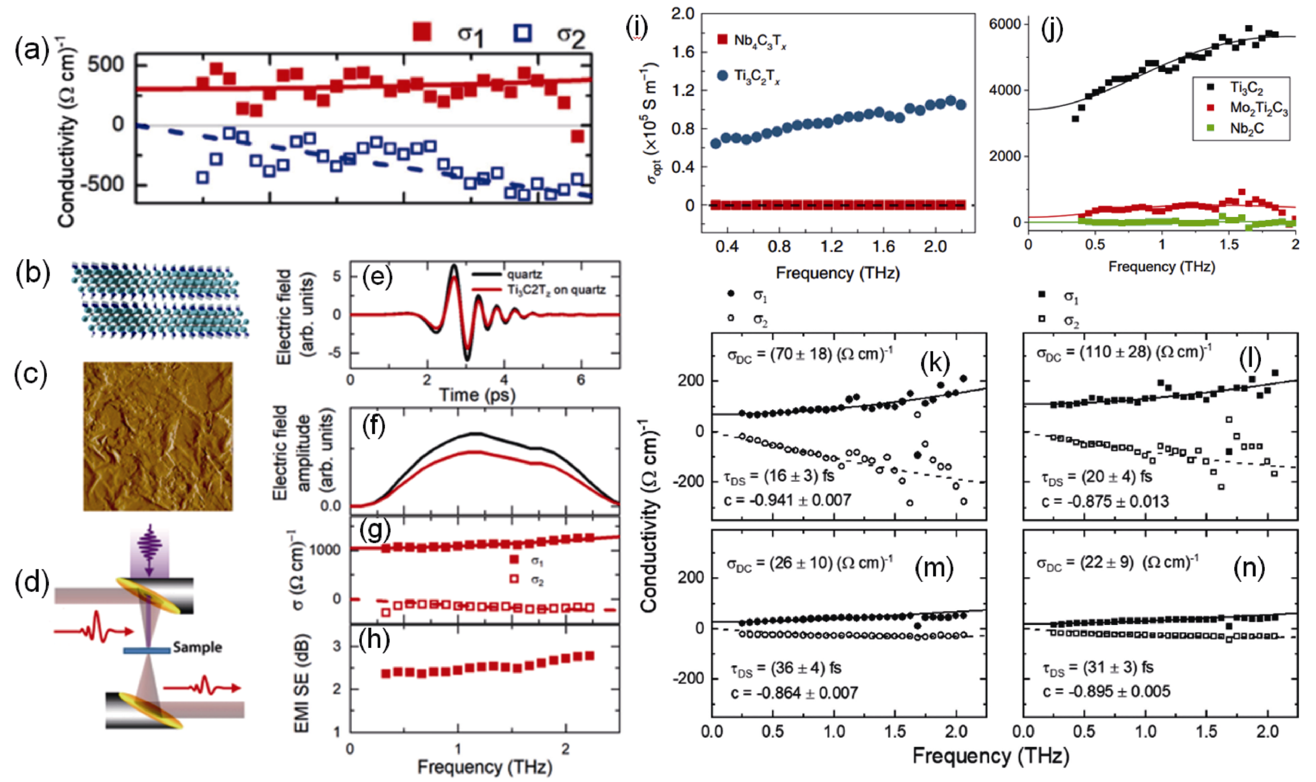

图 5 MXenes 的太赫兹电导响应特性

Fig. 5 Terahertz conductivity characteristics of MXenes

(a) Complex THz conductivity of the 16 nm $Ti_3C_2T_x$ film, and lines-global fitting of the real and imaginary conductivity to the Drude-Smith model (solid red line, fit to σ_1, dashed blue line, fit to σ_2)[60]; (b) Schematic representation of a $Ti_3C_2T_x$ film: five atomic layers thick Ti_3C_2 cores of individual flakes are terminated by –OH, –F, or =O groups; (c) 2 μm by 2 μm AFM micrograph of a 25 nm thick $Ti_3C_2T_x$ film; (d) THz spectroscopy experiment; (e) THz probe pulse transmitted through the substrate with a $Ti_3C_2T_x$ film; (f) Corresponding THz electric field amplitude; (g) THz complex conductivity (solid symbols represent real and open symbols represent imaginary conductivity components; lines show a global fit of both components to the Drude-Smith model); (h) EMI SE calculated from data in (e)[62]; (i) Terahertz conductivity of $Nb_4C_3T_x$ and $Ti_3C_2T_x$ MXene thin films; (j) Real component of THz conductivity in three MXenes films ($Ti_3C_2T_x$, $Mo_2Ti_2C_3T_x$ and Nb_2CT_x) measured by the THz time-domain spectroscopy. Symbols are experiment data, and lines are fit to the Drude-Smith model. Extrapolation 0 THz yield static, DC conductivity[63-64]; TDS of (k, l) $Mo_2Ti_2C_3T_z$ and (m, n) $Mo_2TiC_2T_x$ (k, m) as deposited and (l, n) after a mild 200 ℃ vacuum annealing$_z$. Solid symbols represent real and open symbols represent imaginary conductivity, with lines showing global fits of both the real and imaginary conductivity to the Drude-Smith model with parameters σ_{DC}, τ_{DS} and c indicated on individual panels[61] (Reprinted from Ref. [60] with permission, Copyright 2022, IOP Publishing; Reprinted from Refs. [61-62] with permission, Copyright 2020, American Chemical Society; Reprinted from Ref. [63] with permission, Copyright 2022, Wiley-VCH.; Reprinted from Ref. [64] with permission, Copyright 2022, Springer Nature)

表 2 MXenes 基于 Drude-Smith 模型的太赫兹电子弛豫时间与背散射拟合参数[60-62, 64-65]

Table 2 MXenes fitting parameters for terahertz electron relaxation time and backscattering based on the Drude-Smith model [60-62,64-65]

MXenes	Film fabrication method	Thickness/nm	τ /fs	c	Ref.
$Ti_3C_2T_x$ (MILD)	Interfacial thin film technology	16	6±1	–0.97±0.03	[60]
$Ti_3C_2T_x$ (MILD)	Interfacial thin film technology	25±5	19±1	–0.68	[62]
$Ti_3C_2T_x$	/	/	67±3	～–0.65	[64]
		3.0±0.2	9.62±0.1	–0.82±0.0015	
		6.4±0.3	10.61±0.2	–0.79±0.0016	
		8.0±0.7	10.73±0.2	–0.76±0.0019	
Al-$Ti_3C_2T_x$	Self-assemble technology	10.2±0.1	10.98±0.2	–0.72±0.0016	[65]
		11.8±0.5	12.60±0.2	–0.68±0.0013	
		13.3±0.5	12.59±0.1	–0.66±0.0012	
$Mo_2Ti_2C_3T_x$ (HF TBAOH)	Spin-coating technology	~80	16±3	–0.941±0.007	[61]
Annealing-$Mo_2Ti_2C_3T_x$ (HF TBAOH)	Spin-coating technology	~80	20±4	–0.875±0.013	[61]
$Mo_2TiC_2T_x$ (HF TBAOH)	Drop-cast technology	~1300	36±4	–0.864±0.007	[61]
Annealing-$Mo_2TiC_2T_x$ (HF TBAOH)	Drop-cast technology	~1300	31±3	–0.895±0.005	[61]
$Nb_4C_3T_x$-few layer (HF TMAOH)	/	/	52±4	～–0.7	[64]

在一定程度上限制了 MXenes 及其复合物在太赫兹电磁屏蔽与吸收领域的设计与应用。为了进一步理解 MXenes 与太赫兹的相互作用机制，本课题组[65]利用 Marangoni 效应制备自组装 $Ti_3C_2T_x$ 薄膜，并研究了宽谱太赫兹特性随层数的变化。如图 6(a)所示，符合 Drude-Smith 模型的 $Ti_3C_2T_x$ 自组装薄膜在近全太赫兹频段都呈现一致的太赫兹电导率。这与符合 Drude 模型，以石墨烯为代表的快速衰减的太赫兹电导率完全不同[70-72]，说明 $Ti_3C_2T_x$ 是极佳的宽频太赫兹响应材料。通过层数依赖实验发现，$Ti_3C_2T_x$ 的太赫兹电导率随着层数增加而提高，并在近全太赫兹波段实现了理想金属导电薄膜的理论极限 50% 吸收率。此外，该工作还指出材料的高载流子浓度($>\sim10^{21}$ cm^{-3})与极短的载流子弛豫时间($<\sim$15 fs)，是满足太赫兹宽频响应均一的关键因素，部分已报道的 MXenes 处于近全太赫兹均一电导率参数条件附近。这意味着除了 $Ti_3C_2T_x$ 外，其他 MXenes 在太赫兹电磁屏蔽与吸收领域也具有巨大潜力。

在太赫兹频段电磁屏蔽与吸收复合薄膜领域中，大多数工作主要通过调节导电填料 $Ti_3C_2T_x$ 的质量分数，以确保高导电性和/或适当的阻抗。为了推进 MXenes 及其复合层状薄膜作为太赫兹电磁屏蔽与吸收材料在实际场景(如 6G 通信)的应用，研究人员在多个方面开展了大量工作，如屏蔽效能、几何共形能力、耐高低温、耐腐蚀稳定性和高力学特性等[8, 20, 73-75]。如图 7 所示，本课题组[57]利用丙烯腈多元共聚物中氰基的强分子间作用力，实现了 MXene 普适的无衬底选择附着，同时通过调控 MXene 复合物的

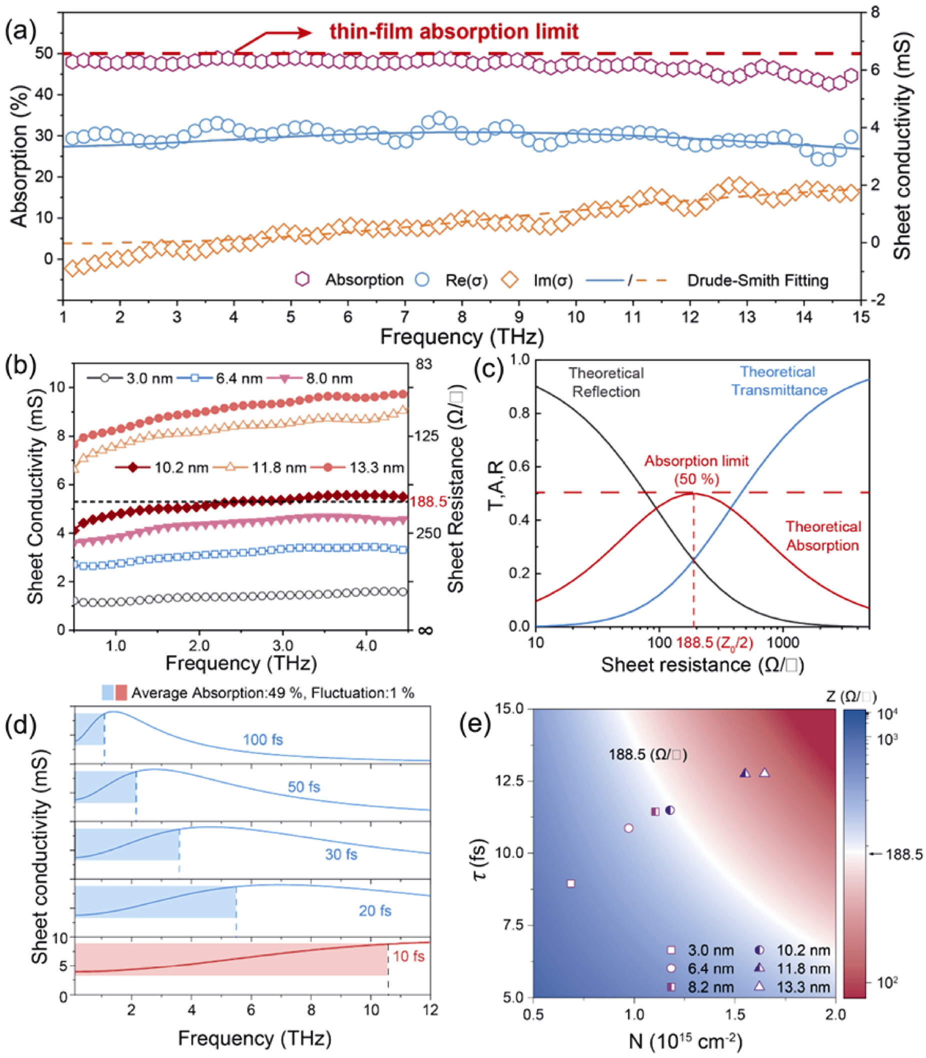

图 6　自组装 $Ti_3C_2T_x$ 薄膜的层数依赖太赫兹响应特性[65]

Fig. 6　Layer-dependent terahertz (THz) conductivity observed in self-assembled $Ti_3C_2T_x$ films[65]

(a) Ultrabroadband terahertz absorption and conductivity of a 17.2 nm $Ti_3C_2T_x$ film measured by an air plasma-based THz-TDS system; (b) Terahertz sheet conductivity and resistance of $Ti_3C_2T_x$ assemblies with different thicknesses for 0.5–4.5 THz; (c) Theoretical transmittance, reflectance and absorption simulated by impedance theory; (d) Conductivity as a function of frequency for a Drude-Smith model with different relaxation times. The shaded bars show the regions where the average absorption is 49% and fluctuation is 1%; (e) Relaxation time τ and sheet carrier concentration N for $Ti_3C_2T_x$ assemblies with different thicknesses. The blue and red colours indicate the higher and lower impedance, respectively (Reprinted from Ref. [65] with permission, Copyright 2023, Springer Nature)

流变特性，赋予大多数平面与非平面构件优异的太赫兹电磁屏蔽效能(38.3 μm, 64.9 dB@0.2~1.6 THz)，从而极大扩展了 MXene 电磁屏蔽与吸收涂料的共性应用范围。此外，对电磁屏蔽与吸收材料而言，环境稳定性也极为重要，然而 MXene 在 H_2O 和 O_2 环境中的稳定性相对较差。2022 年，本课题组[76]提出可以利用材料之间水氧竞争吸附能力差异，并调控 MXene 电荷分布来抑制 MXene 与水氧反应氧化。通过密度泛函理论(Density Functional Theory, DFT)计算比对不同材料在吸附氧气时的电子转移能力来评估其吸附强度，经过研究发现，提纯后的层状膨润土材料对于 O_2 有着极高的吸附能(0.421 eV)，而 $Ti_3C_2O_2$ 的吸附能仅为(0.068 eV)。同时饱和吸附 O_2 的二维膨润土可调控 MXene 表面电荷分布，抑制 MXene 与 O_2 的 d-p 轨道杂化。如图 8 所示，二维膨润土与 Mxene 复合形成的层状薄膜在空气中加热至 400 ℃，仍能保持极强的稳定性和电磁屏蔽性能。此外，2023 年，Feng 等[77]利用水性聚氨酯的高柔韧性和可拉伸性与 MXene 进行复合，得到了一种太赫兹电磁屏蔽性能可随拉伸程度调控的柔性薄膜，在最大拉伸程度下调制深度可达 90%。总体上，符合 Drude-Smith 模型的 MXenes 以其极高的、近全太赫兹频段均一的、层数依赖性的 THz 电导特性，使微米厚度的 MXenes 薄膜能够满足极高近全太赫兹电磁屏蔽特性，纳米厚度的 MXenes 薄膜也能满足接近导电薄膜极限的太赫兹吸收。表 3 总结了近年来用于太赫兹电磁屏蔽与吸收领域的 MXenes 及其复合物的相关研究进展[57, 59, 62, 76, 78-89]。

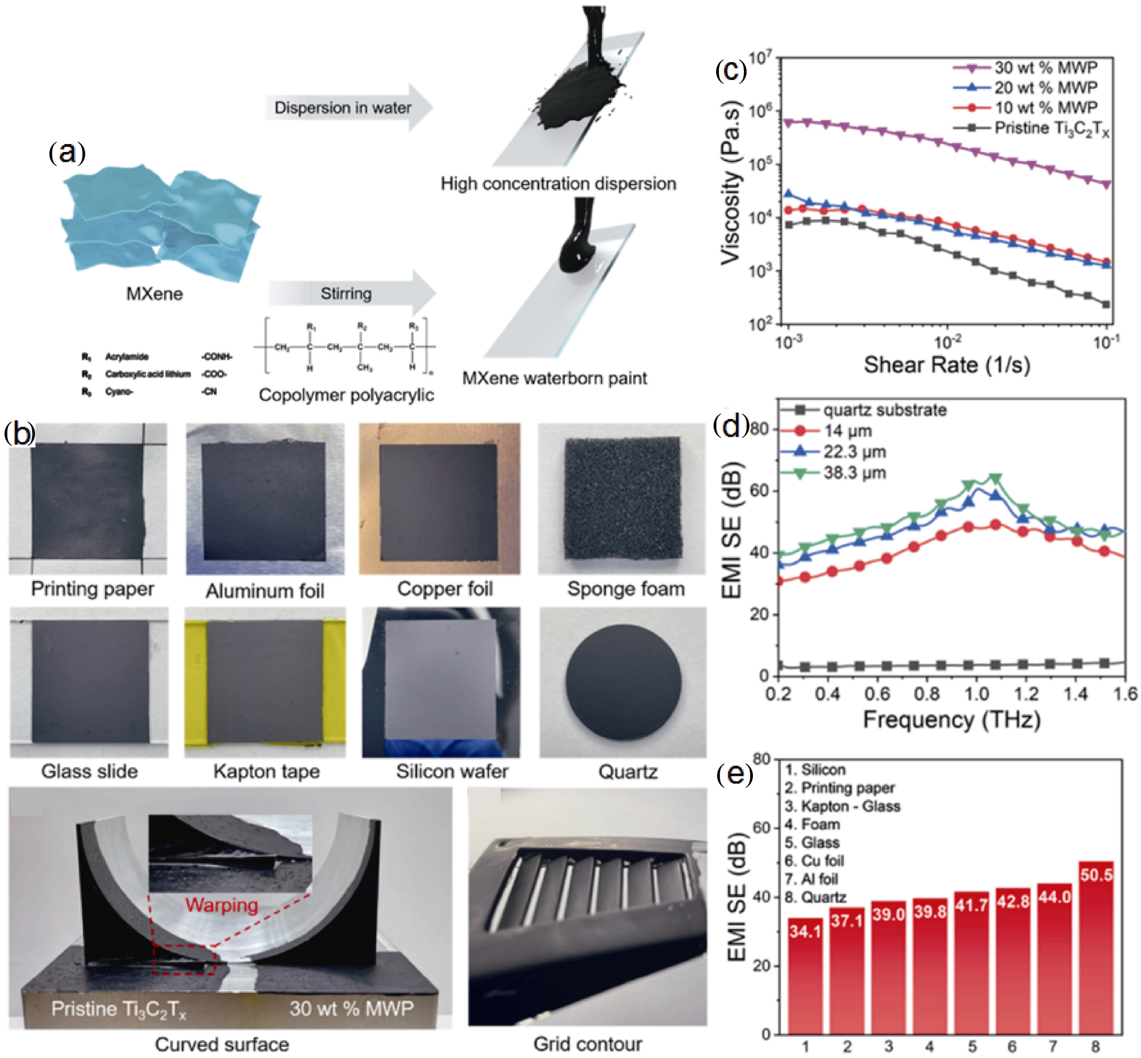

图 7 基底普适性 $Ti_3C_2T_x$ 复合薄膜涂料(MWP)的制备、黏度及太赫兹电磁屏蔽性能[57]

Fig. 7 Synthesis of MWP, and viscosity and EMI SE measurements of different MXene filler content MWP[57]

(a) Schematic of the fabrication of $Ti_3C_2T_x$ water dispersion and $Ti_3C_2T_x$ MXene waterborne paint; (b) Photos of 30% MWP coating on different substrates: printing paper, aluminum foil, copper foil, sponge foam, glass slide, Kapton tape, silicon wafer, and quartz; (c) Viscosity of 40 mg·mL^{-1} MXene water dispersion and MWP with different filler contents; (d) EMI SE *versus* thickness of 30% MWP on quartz; (e) EMI SE at 1 THz of 30% MWP coated on different types of substrates: flexible, rigid, porous (Reprinted from Ref. [57] with permission, Copyright 2021, American Chemical Society)

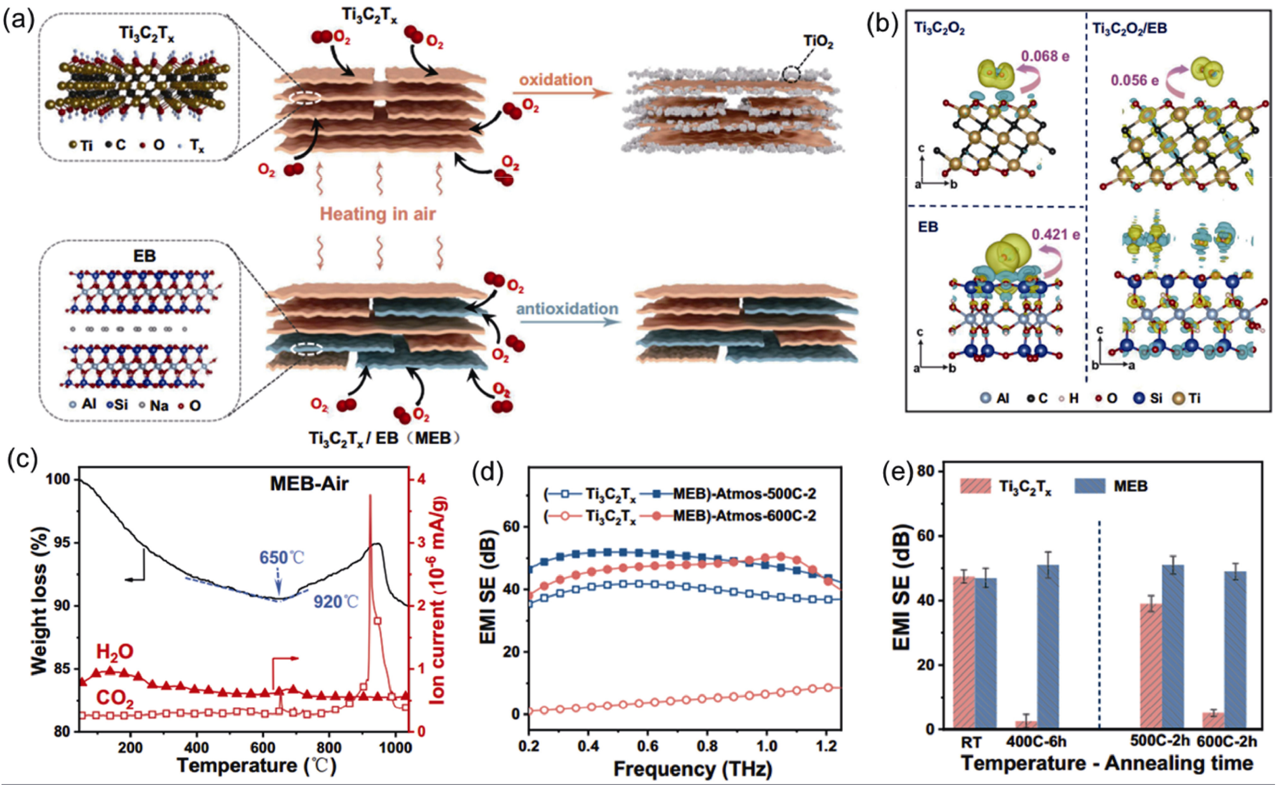

图 8　利用水氧吸附竞争机制的 MXene 与层状蒙脱土耐高温太赫兹电磁屏蔽复合薄膜[76]

Fig. 8　High-temperature terahertz electromagnetic shielding composite film of MXene and layered montmorillonite utilizing a water-oxygen adsorption competition mechanism[76]

(a) Schematic showing the oxidation process of pristine $Ti_3C_2T_x$ (starting from the edge) and suppressed oxidation of MEB under high-temperature annealing with the presence of oxygen; (b) Charge density difference plots for the stable configurations of one O_2 adsorbed on $Ti_3C_2O_2$, EB, and $Ti_3C_2O_2$/EB heterostructure. In the heterostructure, EB is subject to saturated oxygen adsorption. The isosurface level is set to be 0.0002 e/Å^3 except for O_2 adsorbed on EB with a value of 0.0006 e/Å^3. The yellow area indicates charge accumulation, and the green region represents charge depletion; (c) Thermal gravimetric (TG) curves in the air with mass spectrometry analysis (MS) for the atomic mass unit (amu) of 18/H_2O and 44/CO_2 for $Ti_3C_2T_x$ and EB (MEB); (d) EMI SE in 0.2–1.3 THz of $Ti_3C_2T_x$-Atmos-500C-2, 600C-2, and MEB-Atmos-500C-2, 600C-2; (e) Average THz SE of the samples showed in (d) (Reprinted from Ref. [76] with permission, Copyright 2022, Springer Nature)

表 3　MXenes 及其复合材料的太赫兹电磁屏蔽与吸收特性[57, 59, 62, 76, 78-89]

Table 3　Terahertz electromagnetic shielding and absorption properties of MXenes and their composites [57, 59, 62, 76, 78-89]

	Composition	Density/ (g·cm^{-3})	Thickness/ μm	SE/dB	SSE/t/ (dB·cm^2·g^{-1})	Absorption /(RL·dB^{-1})	Frequency band/THz	Ref.
Compact & laminated structure	$Ti_3C_2T_x$	/	0.15	20	/	/	1.0	[59]
	$Ti_3C_2T_x$	ca. 2.39	0.025	~2.5	~7×10^5	/	0.25–2.25	[62]
	$Ti_3C_2T_x$	/	25	55~70	/	/	0.3–0.7	[78]
	Ti_2CT_x/PDMS	/	/	~6	/	/	0.2–3	[79]
	PAN/$Ti_3C_2T_x$/AgNPs	/	3.85	9.11	/	/	0.2–1.2	[80]
	$Ti_3C_2T_x$/copolymer-polyacrylic	/	38.3	64.9	/	/	0.2–1.6	[57]
	PVA/$Ti_3C_2T_x$/MWCNT	/	42	23~36	/	/	0.2–2.0	[81]
	$Ti_3C_2T_x$/extracted bentonite	/	11	47	/	/	0.2–1.3	[76]
	$Ti_3C_2T_x$/ polyaramids	/	20	52.7	/	/	0.2–1.6	[82]
Porous structure	$Ti_3C_2T_x$/GO	/	4000	/	/	37 dB	0.2–2.0	[83]
	Zn^{2+}/$Ti_3C_2T_x$/GO	0.11	85	51	451.0	/	0.2–2.0	[84]
	$Ti_3C_2T_x$/polyurethane	/	2000	/	/	99.99%	0.3–1.65	[85]
	$Ti_3C_2T_x$/PAA/ACC nanoparticle	/	130	45.3	/	23.2	0.2–2.0	[86]
	$Ti_3C_2T_x$/polyurethane/SCA/silica	/	2000	/	/	99.6%	0.3–1.2	[87]
	$Ti_3C_2T_x$/rGO	/	148	~30	/	99.999%	0.37–2.0	[88]
	$Ti_3C_2T_x$/polysiloxane	/	2500	/	/	27.3	0.2–1.4	[89]

4 MXenes 及其复合物多孔材料

相较于电磁屏蔽与吸收薄膜，吸波材料的无序多孔三维骨架作为常用框架也备受关注，无序多孔结构不仅有利于接收更多宽频入射电磁波，也可以在框架内部引起多次反射损耗。为了实现最佳效果，三维骨架的等效阻抗需要与空气阻抗匹配[90-91]。2019 年，南开大学黄毅课题组[83]验证了 $Ti_3C_2T_x$ 与氧化石墨烯的二元复合吸波泡沫在 0.2~2.0 THz 频段具有高达

将 $Ti_3C_2T_x$ 附着在商用发泡聚氨酯上，系统地研究了孔径、MXene 载量、吸波体厚度三个因素对太赫兹吸收性能的影响。在最优化条件下，实现了 99.99%的吸收率。此外，研究人员还观察到 MXene 在多孔骨架表面的连续薄膜与非连续薄膜的特征，并推测随机分布的连续 MXene 薄膜会导致太赫兹波的传输路径更加无序，从而增加内部多重反射损耗。但其内部无序程度与太赫兹波吸收的构效关系，仍无统一的理论解释。因此，如何制备固定的 MXene 多孔结构和调控无序程度，是厘清孔结构、无序程度、电磁 10 所示，

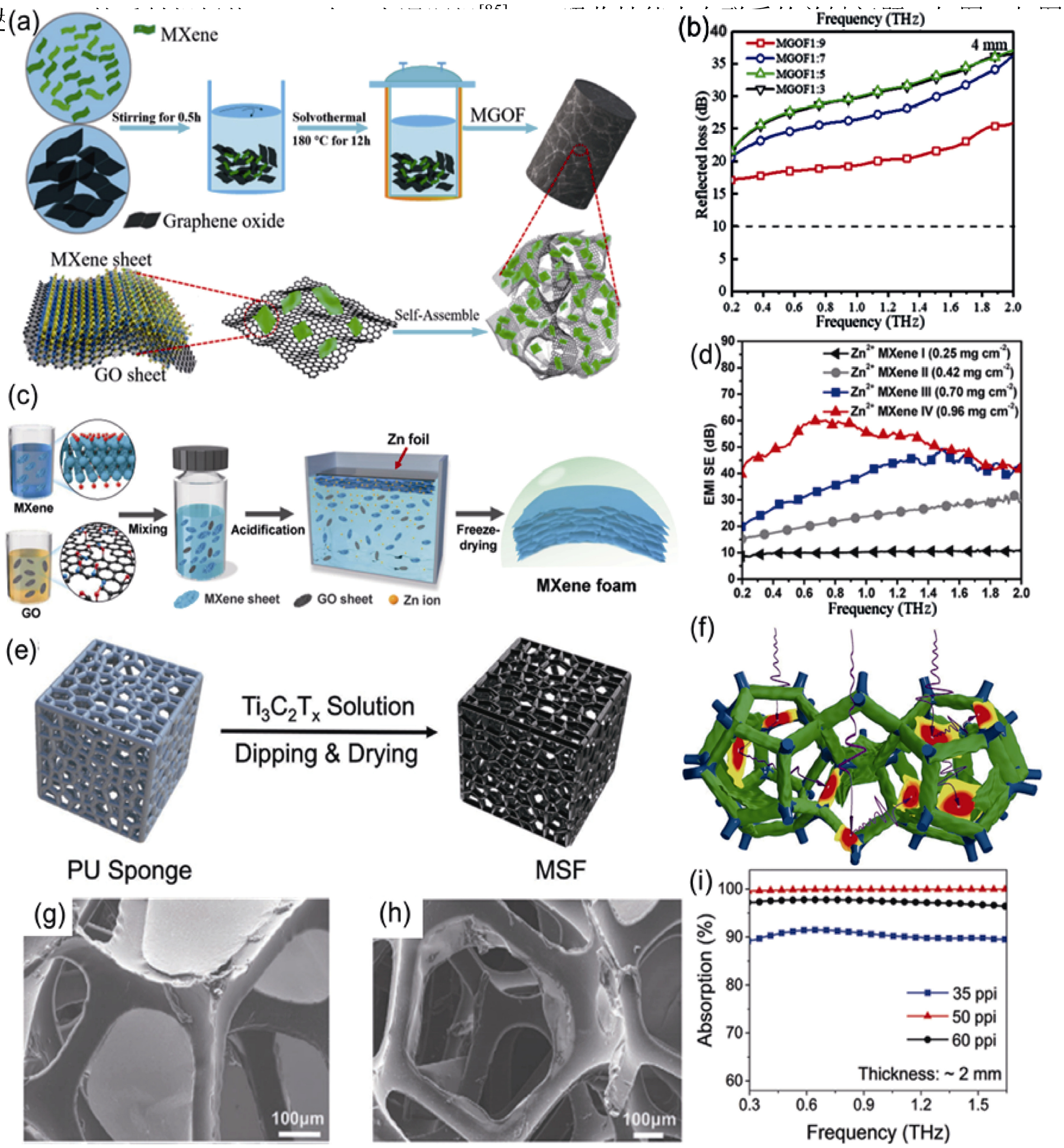

图 9 $Ti_3C_2T_x$ 及其复合多孔吸波体的太赫兹吸收特性

Fig. 9 Terahertz absorption characteristics of $Ti_3C_2T_x$ and its composite porous absorber

(a) Schematic diagram of the MXene/GO foam (MGOF) preparation process; (b) RL curves of 4 mm MGOF with different contents of MXene added to the GO foam[83]; (c) Schematic illustrating the ion-diffusion-induced gelation process; (d) THz EMI shielding effectiveness of the Zn^{2+} MXene-based foams[84]; (e) Schematic illustration of the fabrication of MSF; (f) THz absorption mechanism of MXene filled 3D porous structure with above typical fill state; Two typical filling states: continuous MXene film on pores (g) and/or discontinuous MXene film on skeletons (h); (i) THz absorption by MSF with different pore sizes but fixed 2 mm thickness and (2.8±0.5) mg $Ti_3C_2T_x$ loading[85]
(Reprinted from Ref. [83] and Ref. [84] with permission, Copyright 2019 and 2020, American Chemical Society; Reprinted from Ref. [85] with permission, Copyright 2020, Wiley-VCH GmbH)

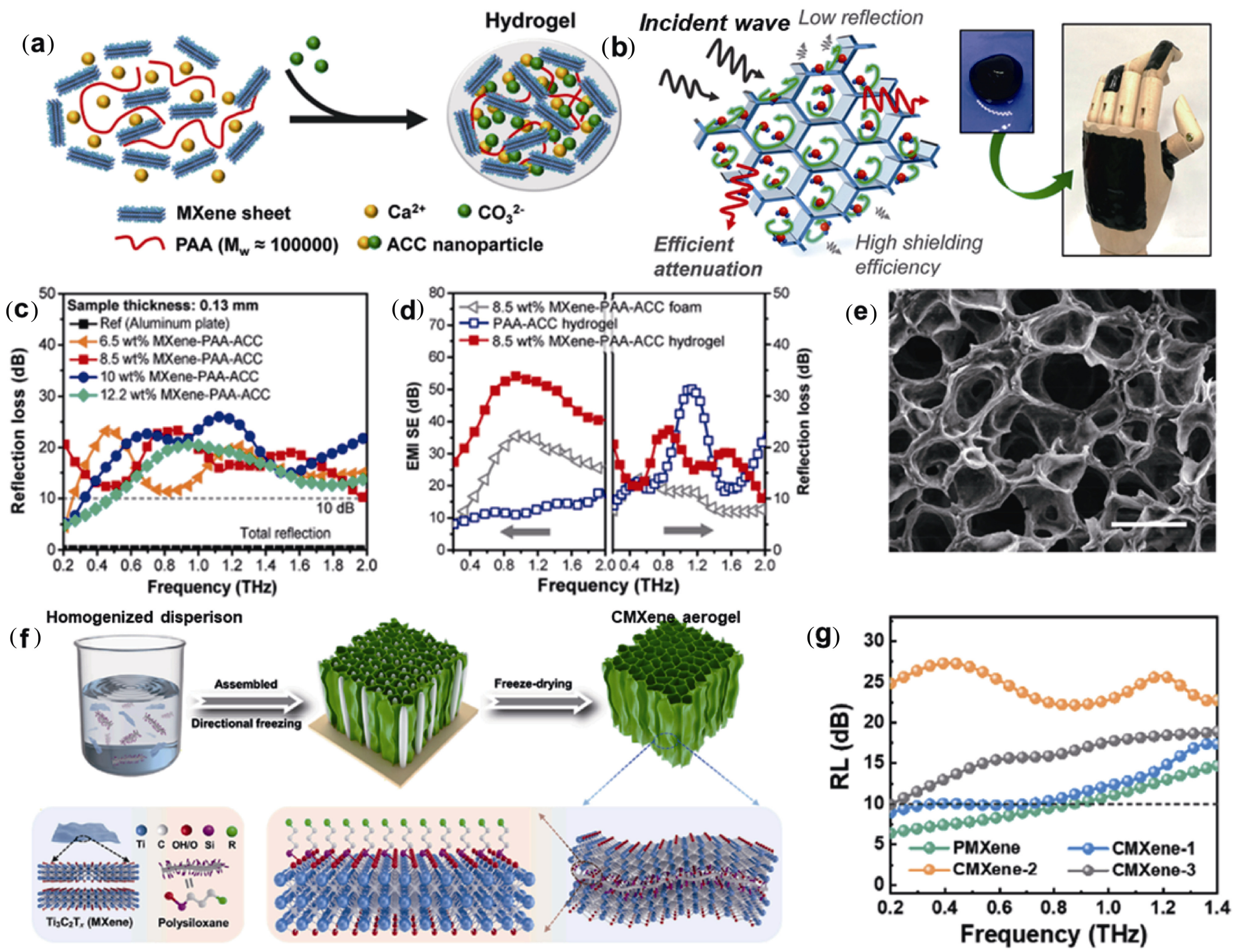

图 10　$Ti_3C_2T_x$ 及其复合多孔水凝胶与定向冷冻干燥气凝胶的太赫兹吸收特性

Fig. 10　Terahertz absorption properties of $Ti_3C_2T_x$ and its composite porous hydrogels and directional freeze-dried aerogels

(a) Schematic illustrating the formation of MXene composite hydrogel; (b) Proposed absorption-dominated EMI shielding mechanism of the MXene composite hydrogel; (c) RL curves of MXene composite hydrogels; (d) Comparison of terahertz EMI shielding and absorption performances between MXene composite hydrogel and reference samples; (e) SEM image of MXene composite hydrogel[86]; (f) Schematic illustration of the fabrication of CMXene; (g) RL curves in THz band of all MXene-based absorbers[89] (Reprinted from Ref. [86] with permission, Copyright 2021, American Chemical Society; Reprinted from Ref. [89] with permission, Copyright 2023, Elsevier B.V.)

研究人员提出了多种方法来构建超轻、超薄、高效的三维 MXene 结构，包括界面组装、水热处理、聚合物辅助组装、模板法、3D 打印技术和冷冻铸造等[83,85-87, 89, 90, 92-93]。例如 Zhu 等[86]报道的一种仅 85 μm 厚的水凝胶型 $Ti_3C_2T_x$/PAA/ ACC 复合电磁屏蔽与吸收材料，具有高达 20 dB 的反射损耗，不仅能够保形黏附在任意复杂几何形状的物体上，还能快速从损坏中恢复，具有广泛的应用前景，特别是在可穿戴电子产品与人造电磁隐身皮肤领域。尽管已有大量研究提出了多种构建多孔 MXene 骨架的方法，但是规则多孔结构的仿真计算复杂度极高。目前鲜有关于太赫兹波段多孔结构孔径、几何构型与阻抗等参数的研究报道，也缺乏指导性的多孔模板，需要进一步开展研究以解决上述挑战。

5 结论与展望

综上所述，研究太赫兹电磁屏蔽与吸收材料对于确保太赫兹探测、成像、通信设备的正常运行至关重要。MXenes 材料以其均一的太赫兹宽频电导、超轻和极强的加工性成为太赫兹电磁屏蔽与吸收优选材料。但是，从实际应用角度来看，MXenes 仍面临几大挑战需要克服:

1)可持续与环境友好的单层 MXenes 制备方法还需进一步探索。传统的湿法刻蚀所用盐酸与氢氟酸对自然环境与人身安全有着极大的风险，熔融盐刻蚀法虽然环境友好、制备快速，但是高温处理会造成剥离单层 MXenes 非常困难。

2)提升 MXenes 的极端环境稳定性，如耐腐蚀、耐高低温、耐强电离辐射等，用以扩展 MXenes 太赫兹屏蔽与吸收材料在太赫兹辐射与探测、6G 通信、航空航天领域的应用。

3)基于 MXenes 的太赫兹电磁屏蔽与吸收最优化构型，目前仍缺乏相关的系统性理论仿真验证。此外，太赫兹宽频响应测试主要依赖于太赫兹时域光谱，该方法并不完全适用多孔材料或非平整样品，其散射特性并不能被完全提取，因此需要完善相关测试方法与测试系统。随着 MXenes 与太赫兹相互作用机制的深入挖掘，合成方式与环境稳定性的进一步发展，MXenes 及其复合物的宽带太赫兹电磁屏蔽与吸收材料将会有更广阔的应用场景。

参考文献:

[1] KULESA C. Terahertz spectroscopy for astronomy: from comets to cosmology. *IEEE Transactions on Terahertz Science and Technology*, 2011, **1(1):** 232.

[2] CHRISTOPHER K. WALKER. Terahertz Astronomy. Boca Raton: Taylor & Francis Group, LLC, 2016: 261–282.

[3] SENGUPTA K, NAGATSUMA T, MITTLEMAN D M. Terahertz integrated electronic and hybrid electronic-photonic systems. *Nature Electronics*, 2018, **1(12):** 622.

[4] LIU J L, DAI J M, CHIN S L, *et al.* Broadband terahertz wave remote sensing using coherent manipulation of fluorescence from asymmetrically ionized gases. *Nature Photonics*, 2010, **4(9):** 627.

[5] BAXTER J B, GUGLIETTA G W. Terahertz spectroscopy. *Analytical Chemistry*, 2011, **83(12):** 4342.

[6] SUNG S J, SELVIN S, BAJWA N, *et al.* THz imaging system for *in vivo* human cornea. *IEEE Transactions on Terahertz Science and Technology*, 2018, **8(1):** 27.

[7] YAN Z Y, ZHU L G, MENG K, *et al.* THz medical imaging: from *in vitro* to *in vivo*. *Trends in Biotechnology*, 2022, **40(7):** 816.

[8] DANG S P, AMIN O, SHIHADA B, *et al.* What should 6G be? *Nature Electronics*, 2020, **3(1):** 20.

[9] RIKKINEN K, KYOSTI P, LEINONEN M E, *et al.* THz radio communication: link budget analysis toward 6G. *IEEE Communications Magazine*, 2020, **58(11):** 22.

[10] SERGHIOU D, KHALILY M, BROWN T W C, *et al.* Terahertz channel propagation phenomena, measurement techniques and modeling for 6G wireless communication applications: a survey, open challenges and future research directions. *IEEE Communications Surveys and Tutorials*, 2022, **24(4):** 1957.

[11] KUMAR A, GUPTA M, PITCHAPPA P, *et al.* Phototunable chip-scale topological photonics: 160 Gbps waveguide and demultiplexer for THz 6G communication. *Nature Communications*, 2022, **13:** 5404.

[12] YANG Y H, YAMAGAMI Y, YU X B, *et al.* Terahertz topological photonics for on-chip communication. *Nature Photonics*, 2020, **14(7):** 446.

[13] JASON F, LARRY S, GASIEWSK A J. A near-millimeter wave interferometric radar. 2013 IEEE Radar Conference, Ottawa, 2013**:** 1–5.

[14] ZHANG B, PI Y Y, LI J. Terahertz imaging radar with inverse aperture synthesis techniques: system structure, signal processing, and experiment results. *IEEE Sensors Journal*, 2015, **15(1):** 290.

[15] CARIS M, STANKO S, PALM S, *et al.* 300 GHz radar for high resolution SAR and ISAR applications. 2015 16th International Radar Symposium (IRS), Dresden, 2015**:** 577–580.

[16] DICKINSON J C, THOMAS M G, WALDMAN J. High resolution imaging using 325 GHz and 1.5 THz transceivers. 15th International Symposium on Space Terahertz Technology, Northampton, 2004**:** 373–380.

[17] HEMMAT M, AYARI S, MIČICA M, *et al.* Layer-controlled nonlinear terahertz valleytronics in two-dimensional semimetal and semiconductor $PtSe_2$. *InfoMat*, 2023, **5(11):** e12468.

[18] DONG Z, YU W, ZHANG L, *et al.* Wafer-scale patterned growth of type-II Dirac semimetal platinum ditelluride for sensitive room-temperature terahertz photodetection. *InfoMat*, 2023, **5(5):** e12403.

[19] LIU B, ZHANG X, DU J, *et al.* Synergistic-engineered van der Waals photodiodes with high efficiency. *InfoMat*, 2022, **4(3):** e12282.

[20] IQBAL A, SAMBYAL P, KOO C M. 2D MXenes for electromagnetic shielding: a review. *Advanced Functional Materials*, 2020, **30(47):** 2000883.

[21] LIU L, DAS A, MEGARIDIS C M. Terahertz shielding of carbon nanomaterials and their composites—a review and applications. *Carbon*, 2014, **69:** 1.

[22] CHE R C, PENG L M, DUAN X F, *et al.* Microwave absorption enhancement and complex permittivity and permeability of Fe encapsulated within carbon nanotubes. *Advanced Materials*, 2004, **16(5):** 401.

[23] SUN H, CHE R C, YOU X, *et al.* Cross-stacking aligned carbon-nanotube films to tune microwave absorption frequencies and increase absorption intensities. *Advanced Materials*, 2014, **26(48):** 8120.

[24] LIU Q H, CAO Q, BI H, *et al.* CoNi@SiO_2@TiO_2 and CoNi@Air@TiO_2 microspheres with strong wideband microwave absorption. *Advanced Materials*, 2016, **28(3):** 486.

[25] CHE R C, ZHI C Y, LIANG C Y, *et al.* Fabrication and microwave absorption of carbon nanotubes/$CoFe_2O_4$ spinel nanocomposite. *Applied Physics Letters*, 2006, **88(3):** 033105.

[26] SOKOL M, NATU V, KOTA S, *et al.* On the chemical diversity of the MAX phases. *Trends in Chemistry*, 2019, **1(2):** 210.

[27] DING H M, LI Y B, LI M, *et al.* Chemical scissor–mediated structural editing of layered transition metal carbides. *Science*, 2023, **379(6637):** 1130.

[28] WEI Y, ZHANG P, SOOMRO R A, *et al.* Advances in the synthesis of 2D MXenes. *Advanced Materials*, 2021, **33(39):** e2103148.

[29] MOHAMMADI A V, ROSEN J, GOGOTSI Y. The world of two-dimensional carbides and nitrides (MXenes). *Science*, 2021, **372(6547):** eabf1581.

[30] IQBAL A, SHAHZAD F, HANTANASIRISAKUL K, *et al.* Anomalous absorption of electromagnetic waves by 2D transition metal carbonitride $Ti_3C_NT_x$ (MXene). *Science*, 2020, **369(6502):** 446.

[31] FAISAL S, MOHAMED A, CHRISTINE B, *et al*. Electromagnetic interference shielding with 2D transition metal carbides (MXenes). *Science*, 2016, **353(6304):** 1137.

[32] WU Z C, CHENG H W, JIN C, *et al.* Dimensional design and core-shell engineering of nanomaterials for electromagnetic wave absorption. *Advanced Materials*, 2022, **34(11):** 2107538.

[33] LU J, LI X, HWANG H Y, *et al.* Coherent two-dimensional terahertz magnetic resonance spectroscopy of collective spin waves. *Physical Review Letters*, 2017, **118(20):** 207204.

[34] CASPERS C, GANDHI V P, MAGREZ A, *et al.* Sub-terahertz spectroscopy of magnetic resonance in $BiFeO_3$ using a vector network analyzer. *Applied Physics Letters*, 2016, **108(24):** 241109**.**

[35] BITZER A, MERBOLD H, THOMAN A, *et al.* Terahertz near-field imaging of electric and magnetic resonances of a planar metamaterial. *Optics Express*, 2009, **17(5):** 3826.

[36] YEN T J, PADILLA W J, FANG N, *et al.* Terahertz magnetic response from artificial materials. *Science*, 2004, **303(5663):** 1494.

[37] WATTS C M, LIU X L, PADILLA W J. Metamaterial electromagnetic wave absorbers. *Advanced Materials*, 2012,

24(23): 98.

[38] YOUJI K. Electromagnetic wave absorbers detailed theories and applications. Hoboken: John Wiley & Sons, Inc, 2019: 5–20.

[39] SALISBURY W W. Absorbent body for electromagnetic waves. US2599944. 1952-06-10.

[40] LI H, LI F F, FAN D G, *et al.* Wideband electromagnetic absorber based on array of parallel-plate waveguide. 2017 International Conference on Electromagnetics in Advanced Applications (Iceaa), 2017**:** 1224–1226.

[41] COSTA F, MONORCHIO A. A frequency selective radome with wideband absorbing properties. *IEEE Transactions on Antennas and Propagation*, 2012, **60(6):** 2740.

[42] JI B, FAN S W, KOU S J, *et al.* Microwave absorption properties of multilayer impedance gradient absorber consisting of $Ti_3C_2T_x$ MXene/polymer films. *Carbon*, 2021, **181:** 130.

[43] ZUO Y X, SU X R, LI X W, *et al.* Multimaterial 3D-printing of graphene/LiZnFeO and graphene/carbonyl iron composites with superior microwave absorption properties and adjustable bandwidth. *Carbon*, 2020, **167:** 62.

[44] DEWITT B T, BURNSIDE W D. Electromagnetic scattering by pyramidal and wedge absorber. *IEEE Transactions on Antennas and Propagation*, 1988, **36(7):** 971.

[45] JOHNK R T, ONDREJKA A, TOFANI S, *et al.* Time-domain measurements of the electromagnetic backscatter of pyramidal absorbers and metallic plates. *IEEE Transactions on Electromagnetic Compatibility*, 1993, **35(4):** 429.

[46] SHEN Z, LI S, XU Y, *et al.* Three-dimensional printed ultrabroadband terahertz metamaterial absorbers. *Physical Review Applied*, 2021, **16(1):** 014066.

[47] WANG C Q, SWEENEY W R, STONE A D, *et al.* Coherent perfect absorption at an exceptional point. *Science*, 2021, **373(6560):** 1261.

[48] SLOBODKIN Y, WEINBERG G, HORNER H, *et al.* Massively degenerate coherent perfect absorber for arbitrary wavefronts. *Science*, 2022, **377(6609):** 995.

[49] BARANOV D G, KRASNOK A, SHEGAI T, *et al.* Coherent perfect absorbers: linear control of light with light. *Nature Reviews Materials*, 2017, **2(12):** 17064.

[50] LI S C, LUO J, ANWAR S, *et al.* Broadband perfect absorption of ultrathin conductive films with coherent illumination: superabsorption of microwave radiation. *Physical Review B*, 2015, **91(22):** 220301.

[51] PAPAIOANNOU M, PLUM E, VALENTE J, *et al.* Two-dimensional control of light with light on metasurfaces. *Light-Science & Applications*, 2016, **5:** e16070.

[52] NARIMANOV E E, KILDISHEV A V. Optical black hole: broadband omnidirectional light absorber. *Applied Physics Letters*, 2009, **95(4):** 041106.

[53] LEONARD M H, KEITH A S. Integrating spheres for mid- and near infrared reflection spectroscopy. Chichester: John Wiley & Sons Ltd, 2002.

[54] WANG C L, CHIU C P, HUANG P J, *et al.* High-performance 1–10 THz integrating sphere. *Applied Optics*, 2021, **60(13):** 3784.

[55] WU Y, BAI Y. Radar cross section measurement in terahertz. 2016 Progress in Electromagnetics Research Symposium (Piers), 2016**:** 2991–2994.

[56] IWASZCZUK K, HEISELBERG H, JEPSEN P U. Terahertz radar cross section measurements. *Optics Express*, 2010, **18(25):** 26399.

[57] WAN H J, LIU N, TANG J, *et al.* Substrate-independent $Ti_3C_2T_x$ MXene waterborne paint for Terahertz absorption and shielding. *ACS Nano*, 2021, **15(8):** 13646.

[58] JHON Y I, SEO M, JHON Y M. First-principles study of a MXene terahertz detector. *Nanoscale*, 2018, **10(1):** 69.

[59] CHOI G, SHAHZAD F, BAHK Y M, *et al.* Enhanced terahertz shielding of MXenes with nano-metamaterials. *Advanced Optical Materials*, 2018, **6(5):** 1701076.

[60] LI G J, KUSHNIR K, DONG Y C, *et al.* Equilibrium and non-equilibrium free carrier dynamics in 2D $Ti_3C_2T_x$ MXenes: THz spectroscopy study. *2D Materials*, 2018, **5(3):** 035043.

[61] LUI G, NATU V, SHI T, *et al.* Two-dimensional MXenes $Mo_2Ti_2C_3T_z$ and $Mo_2TiC_2T_z$: microscopic conductivity and dynamics of photoexcited carriers. *ACS Applied Energy Materials*, 2020, **3(2):** 1530.

[62] LI G J, AMER N, HAFEZ H A, *et al.* Dynamical control over Terahertz electromagnetic interference shielding with 2D $Ti_3C_2T_y$ MXene by ultrafast optical pulses. *Nano Letters*, 2020, **20(1):** 636.

[63] COLIN-ULLOA E, FITZGERALD A, MONTAZERI K, *et al.* Ultrafast spectroscopy of plasmons and free carriers in 2D MXenes. *Advanced Materials,* 2023, **35(8)**: e2208659.

[64] ZHENG W, SUN B, LI D, *et al.* Band transport by large Fröhlich polarons in MXenes. *Nature Physics*, 2022, **18(5):** 544.

[65] ZHAO T, XIE P Y, WAN H J, *et al.* Ultrathin MXene assemblies approach the intrinsic absorption limit in the 0.5–10 THz band. *Nature Photonics*, 2023, **17(7):** 622.

[66] LI Y B, SHAO H, LIN Z F, *et al.* A general Lewis acidic etching route for preparing MXenes with enhanced electrochemical performance in non-aqueous electrolyte. *Nature Materials*, 2020, **19(8):** 894.

[67] MATHIS T S, MALESKI K, GOAD A, *et al.* Modified MAX phase synthesis for environmentally stable and highly conductive Ti_3C_2 MXene. *ACS Nano*, 2021, **15(4):** 6420.

[68] KIM Y J, KIM S J, SEO D, *et al.* Etching mechanism of monoatomic aluminum layers during MXene synthesis. *Chemistry of Materials*, 2021, **33(16):** 6346.

[69] MICHALOWSKI P P, ANAYEE M, MATHIS T S, *et al.* Oxycarbide MXenes and MAX phases identification using monoatomic layer-by-layer analysis with ultralow-energy secondary-ion mass spectrometry. *Nature Nanotechnology*, 2022, **17(11):** 1192.

[70] BALCI O, POLAT E O, KAKENOV N, *et al.* Graphene-enabled electrically switchable radar-absorbing surfaces. *Nature Communications*, 2015, **6:** 6628.

[71] PHAM P H Q, ZHANG W D, QUACH N V, *et al.* Broadband impedance match to two-dimensional materials in the terahertz domain. *Nature Communications*, 2017, **8:** 2233.

[72] STEN J C E, KOIVISTO P K. Optimum transparent absorbers of electromagnetic waves. *IEEE Transactions on Electromagnetic Compatibility*, 2008, **50(4):** 1011.

[73] THOMASSIN J M, JEROME C, PARDOEN T, *et al.* Polymer/carbon based composites as electromagnetic interference (EMI) shielding materials. *Materials Science & Engineering R-Reports*, 2013, **74(7):** 2112.

[74] OLIVEIRA F M, AZADMANJIRI J, WANG X H, *et al.* Structure design and processing strategies of MXene-based materials for electromagnetic interference shielding. *Small Methods*, 2023, **7(7):** 2300112.

[75] WAN S J, LI X, CHEN Y, *et al.* High-strength scalable MXene films through bridging-induced densification. *Science*, 2021, **374(6563):** 96.

[76] LIU N, LI Q Q, WAN H J, *et al.* High-temperature stability in air of $Ti_3C_2T_x$ MXene-based composite with extracted bentonite. *Nature Communications*, 2022, **13:** 5551.

[77] FENG T D, HU Y W, CHANG X, *et al.* Highly flexible $Ti_3C_2T_x$ MXene/waterborne polyurethane membranes for high-efficiency terahertz modulation with low insertion loss. *ACS Applied Materials & Interfaces*, 2023, **15(5):** 7592.

[78] ZOU Q, GUO W Y, ZHANG L, *et al.* MXene-based ultra-thin film for terahertz radiation shielding. *Nanotechnology*, 2020, **31(50):** 505710.

[79] KLAUDIA Z A L, AGNIESZKA S, AGNIESZKA M, *et al*. Terahertz time domain spectroscopy of graphene and MXene polymer composites. *Journal of Applied Polymer Science*, 2020, **138(10):** 49962

[80] ZOU Q, SHI C F, LIU B, *et al.* Enhanced terahertz shielding by adding rare Ag nanoparticles to $Ti_3C_2T_x$ MXene fiber membranes. *Nanotechnology*, 2021, **32(41):** 415204.

[81] HUSSAIN K, MEHBOOB S, AHMAD I, *et al.* Terahertz time-domain spectroscopy of thin and flexible CNT-modified MXene/polymer composites. *Applied Physics A*, 2021, **127(5):** 382.

[82] CHENG Z, CAO Y, WANG R, *et al.* Multifunctional MXene-based composite films with simultaneous terahertz/gigahertz wave shielding performance for future 6G communication. *Journal of Materials Chemistry A*, 2023, **11(11):** 5593.

[83] MA W L, CHEN H H, HOU S Y, *et al.* Compressible highly stable 3D porous MXene/GO foam with a tunable high-performance stealth property in the terahertz band. *ACS Applied Materials & Interfaces*, 2019, **11(28):** 25369.

[84] LIN Z H, LIU J, PENG W, *et al.* Highly stable 3D $Ti_3C_2T_x$ MXene-based foam architectures toward high-performance terahertz radiation shielding. *ACS Nano*, 2020, **14(2):** 2109.

[85] SHUI W C, LI J M, WANG H, *et al.* $Ti_3C_2T_x$ MXene sponge composite as broadband terahertz absorber. *Advanced Optical Materials*, 2020, **8(21):** 2001120.

[86] ZHU Y Y, LIU J, GUO T, *et al.* Multifunctional $Ti_3C_2T_x$ MXene composite hydrogels with strain sensitivity toward absorption-dominated electromagnetic-interference shielding. *ACS Nano*, 2021, **15(1):** 1465.

[87] LUO M, GUO J C, SHUI W C, *et al.* $Ti_3C_2T_x$ MXene-based superhydrophobic broadband terahertz absorber with large pore-size foam architecture. *Advanced Materials Interfaces*, 2022, **10(2):** 2201767.

[88] LI S J, XU S J, PAN K C, *et al.* Ultra-thin broadband terahertz absorption and electromagnetic shielding properties of MXene/rGO composite film. *Carbon*, 2022, **194:** 127.

[89] FEI Y, WANG X Y, WANG F, *et al.* Covalent coupling induced-polarization relaxation in MXene-based terahertz absorber for realizing dual band absorption. *Chemical Engineering Journal*, 2023, **461:** 142049.

[90] WANG L, MA Z, ZHANG Y, *et al.* Polymer-based EMI shielding composites with 3D conductive networks: a mini-review. *SusMat*, 2021, **1(3):** 413.

[91] HORODYNSKI M, KUHMAYER M, FERISE C, *et al.* Anti-reflection structure for perfect transmission through complex media. *Nature*, 2022, **607(7918):** 281.

[92] YUN T, LEE G S, CHOI J, *et al.* Multidimensional $Ti_3C_2T_x$ MXene architectures *via* interfacial electrochemical self-assembly. *ACS Nano*, 2021, **15(6):** 10058.

[93] XUE T T, YANG Y, YU D Y, *et al.* 3D printed integrated gradient-conductive MXene/CNT/polyimide aerogel frames for electromagnetic interference shielding with ultra-low reflection. *Nano-Micro Letters*, 2023, **15(1):** 45.